



Experimental Investigation on the Effects of Swirl on the Exit Turbulent Flow Field of an Unconfined Annular Burner at Isothermal and Reacting Conditions

R. Manikandan, R. Sadanandan and C. Prathap[†]

*Department of Aerospace Engineering, Indian Institute of Space Science and Technology,
Thiruvananthapuram, 695547, India*

[†]Corresponding Author Email: prathapc@iist.ac.in

(Received June 19, 2019; accepted October 13, 2019)

ABSTRACT

The objective was to study the effect of change in swirl intensities, $S=0.4, 0.7$ & 1 of the annular swirling flow on the exit flow field of an unconfined annular swirl burner operated at isothermal (only dry air) and reacting flow (premixed methane air mixture) conditions. Reynolds number at the burner's annular exit based on its hydraulic diameter (D) was kept constant at 4000 . Exit flow field at isothermal conditions was measured using planar particle image Velocimetry rig and processed using commercial software. The percentage decay in the magnitude of peak value of axial velocity obtained from its radial profile at a height of $4D$ from the burner exit with the change in swirl intensity of $1, 0.7, 0.4$ and 0 was $65\%, 55\%, 47.2\%$ and 13.5% . The jet spreading angle was 6.5° for $S=0$, 8.4° for $S=0.4$, 9.8° for $S=0.7$ and 14.2° for $S=1$. Recirculation zone was observed only for $S=0.7$ and 1.0 . The width of the recirculation zone was $3D$ ($S=0.7$) and $3.4D$ ($S=1$) respectively. The normalized reverse mass flow rates estimated were 0.027 for $S=0.7$ and 0.058 for $S=1.0$. The magnitude of turbulence intensities at wake shear layer was much higher than the jet shear layer due to the presence of recirculation zones for $S=0.7$ and 1.0 . The integral length scales calculated were varied in the range of $0.06D-0.18D$ for all swirl intensities. Reaction front was identified by deconvoluting the time mean OH^* chemiluminescence using Abel inversion method. The flame became shorter and wider with increase in swirl number which was in consonance with the observation of increase in size of recirculation flow in the isothermal flow. The equivalence ratios at which the lean blow out observed were $0.58, 0.6$ and 0.62 for $S=0.4, 0.7$ and 1 .

Keywords: Swirling flow; Axial swirl generator; Jet spreading rate; Chemiluminescence; Lean blowout.

1 INTRODUCTION

Swirling jets were successfully used in combustion applications to enhance the flame anchoring stability. Swirl assisted combustion is a complex 3D turbulent reacting flow consisting of recirculation zones resulting in improved flame anchoring stabilization (Bruno and Losurdo, 2007). Swirling jets played a significant role in reducing the length of the diffusion flame due to increased mixing of fuel and oxidizer ensuing high burning efficiency (Chigier and Beér, 1964). Chigier and Chervinsky (1967) measured the velocity profile at the exit of a swirl burner (tangential entry type) with varying swirling intensity from weak to strong. From that information, they estimated the jet spread rate and the reverse mass flow rate. Syred *et al.* (1971) measured the temperature using Pt/Pt-Rh thermocouple and velocity field using constant temperature hot wire anemometer at the exit of a tangential type swirl

burner which deflected the flow corresponding to a swirl number of 2.2 . They concluded that the size and shape of the recirculation zones in the hot and cold states are similar suggesting that the aerodynamic forces predominate and hence the isothermal flow field measurements at the exit of a burner is sufficient enough to estimate the size and shape of the recirculation zone under hot conditions too. Warda *et al.* (1999b) explained that the exit flow field of an annular axial jet can be divided into three different zones such as initial merging zone, intermediate and final merging zones.

Vanierschot and Bulck (2008) presented an extensive study on the influence of swirl on the initial region of an annular jet using stereo PIV. They reported that the concentric central tube of the burner acts as a bluff body to the flow and resulted in a central recirculation zone downstream to it. Later, they introduced swirling motion to the flow

gradually using swirl generators with axial vanes. They observed that even at low swirl intensities, the structure of the CRZ changed to a toroidal recirculation zone leading to entrainment of jet fluid near the apex. At intermediate swirls, they observed vortex breakdown bubble appearing downstream of CRZ and it moves upstream with increased swirl. At high swirl, the CRZ and breakdown bubble merged and resulting in a complex and highly anisotropic flow field. Alekseenko *et al.* (2011) used stereo PIV, CH* Chemiluminescence techniques to study the turbulent flow structure of lifted non-swirling and swirling premixed propane air flames. For non-swirling case, they mentioned that the possible reason for the lifted flame stabilization is due to the interaction of ring-like vortices with the flame front. Another important observation was that the thermal expansion effect did not affect the flow structure of the lifted flame as the flow field data were same for both the isothermal and reacting flow conditions. Kim *et al.* (2009) used PIV, OH chemiluminescence and gas analyzers to measure the velocity field, reaction front and also the emission levels at the exit of an annular swirl burner operated at a power rating of 5.81 kW for different swirler vane angles of 30, 45 and 60. They used a binary gas mixture comprising of methane and hydrogen. They concluded that the reactivity of the mixture also affected the recirculation zone and the corresponding formation of NO_x.

In the premixed flames, flame front is a thin reaction zone where chemical reaction occurs with high local heat release and temperature (Kojima *et al.* 2005). Hence, in reaction front, OH radicals get formed undergo excitation/ de-excitation resulting in chemiluminescence emission. Therefore, OH* emissions from reaction front can be used as a marker to track flame front.

Even though, quite handful of studies available on the swirling turbulent flows, still owing to its degree of complexity, more experimental data are required for improving both isothermal and reacting flow simulations. Introduction of swirl and its effect on enhancing turbulence was also studied. Hence, the objective of the present work was to experimentally investigate the effect of swirl on the turbulent flow field at isothermal conditions using 2D Particle Image Velocimetry (PIV). The desired characteristics of turbulent swirling flow field such as turbulence intensities, jet spread angle, reverse mass flow rate and integral length scales were calculated. To identify the flame front at reacting flow conditions, OH* chemiluminescence technique was used.

2 USEFULL DEFINITIONS

In this section, the definitions of important characteristics of turbulent swirling flow estimated from the measured flow field data are presented.

2.1 Jet Spreading Rate

The important parameters used to characterize the free jets are spreading rate and spreading angle ($\alpha_{1/2}$)

(Turns, 2000). Liang and Maxworthy (2005) mentioned that in the case of free swirling annular jets, the centreline velocity used for estimating the jet half width in the round jet can be replaced by the maximum value of the velocity estimated from the radial profile of axial velocities at a given axial location.

2.2 Integral Length Scale

The integral length scales can be estimated from the measured axial and radial components of the velocity fluctuation. As the present work dealt with the study of flow field of a burner, the axial component of velocity was much more important than the radial component in order to anchor the flame. Hence, the length scales were estimated only from the axial components of the measured flow field data. The length scales information at isothermal conditions can be useful in the estimation of turbulent Reynolds number, eddy dissipation rate, etc. Length scales can be deduced from the correlation coefficient by using Taylor's hypothesis (Liang & Maxworthy, 2005). Correlation coefficient was calculated using Eq. 1).

$$R_{ij}(\vec{x}, \vec{r}) = \frac{\overline{u'_i(\vec{x})u'_j(\vec{x}+\vec{r})}}{u'_{i,rms}(\vec{x})u'_{j,rms}(\vec{x}+\vec{r})} \quad (1)$$

where u'_i is an instantaneous velocity component i , \vec{x} reference point at which the velocity u'_i is measured. \vec{r} is the vector of displacement from the reference point at which the velocity u'_j is measured, $u'_{i,rms}$ and $u'_{j,rms}$ are the root mean square fluctuation velocities at the respective locations. The correlation coefficient R_{ij} is a function of spatial location \vec{x} in the radial direction and displacement, \vec{r} . Then, the integral length scale was estimated from the correlation coefficient using Eq. 2)

$$L_{ij,k}(\vec{x}) = \frac{1}{2} \int_{-\infty}^{\infty} R_{ij}(\vec{x}, r_k) dr_k \quad (2)$$

3 EXPERIMENTAL RIG

In this section, the details of the present experimental rig are explained.

3.1 Burner Rig

The design of the present gaseous fuelled premixed swirl-flame burner used for the current research was adopted from Singh and Chander (2014). The schematic of the annular swirl burner is shown in Fig. 1. The swirl burner consists of four concentric tubes with an annular gap of 8 mm between them. In the present research, only the annular space between Tube 2 with an outer diameter of 45 mm and Tube 3 with an inner diameter of 57 mm was used. Axial swirlers were used. The outer and hub diameters of the designed swirlers were 57 mm and 45 mm respectively in order to fit it into the annular space of the burner. The burner had an annular exit nozzle with an inner diameter and an outer diameter of 10 mm and 25 mm respectively. The hydraulic diameter (D) of the annular regime at the nozzle exit was 15mm.

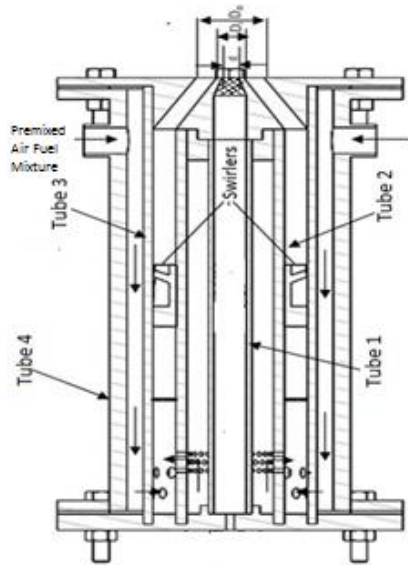


Fig. 1. Burner sectional view.

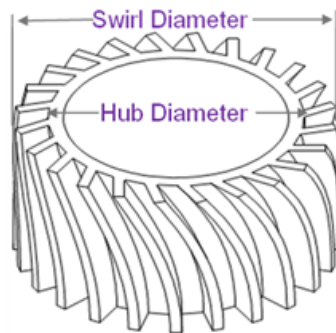


Fig. 2. CAD diagram of Axial vane swirl generator.

The axial swirlers with curved vanes having outer and hub diameters of 57 mm and 45mm for different swirl intensities of 0.4, 0.7 and 1.0 were designed. First, the angle of vanes was estimated using Eq. 1 as reported in Beer and Chigier (1983).

$$S = \frac{G_t}{RG_x} = \frac{2}{3} \left(\frac{1 - (R_h/R)^3}{1 - (R_h/R)^2} \right) \tan \theta \quad (3)$$

where S is the swirl intensity, G_t is the axial flux of tangential momentum estimated at swirler outer radius R , G_x is the axial flux of axial momentum, R_h is the radius of hub and θ is the vane angle. Vane angles were 50° , 38° & 24° for $S=1$, 0.7 & 0.4. After finding the vane angle, curved vanes were designed according to Kilik (1976). A schematic of the CAD model of one of the swirlers is shown in Fig. 2.

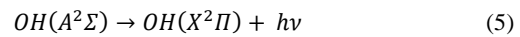
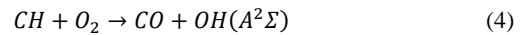
3.2 Particle Image Velocimetry (PIV)

PIV rig consisted of a double pulsed Nd:YAG laser (Spectra Physics). A double-shutter CCD camera (Lavision Imagerpro, 2048×2048 pixels, 14bits) equipped with a focusing lens and a 532 ± 10 nm band pass filter was used for acquiring MIE scattering images. Camera was operated at 5Hz in double shutter mode in synchronization with laser. Thin laser sheet (< 1 mm) was created using sheet optics. Pulse energy of 12.5 mJ at 532 nm was used for

present measurements. The air flow was seeded with olive oil particles (SMD=8 micrometers) to illuminate the flow field with the laser sheet. The duration between the two laser pulses was varied between $55\mu s$ to $75\mu s$ according to the need. The field of view was 45 mm (width) \times 60 mm (height). In the present study, for all the studied operating conditions, the image was recorded for a certain minimum duration of 95s at 5 Hz to obtain the statistical time average velocity data and turbulent characteristics of the present turbulent swirl flow at a Reynolds number of 4000.

3.3 OH* Chemiluminescence

Earlier investigations in the study of reacting flow with gaseous fuels have reported that the intensity of the OH* emissions is directly related to the reaction rate or heat release rate (Kojima *et al.* 2005). So, by capturing the OH* emissions (integrated along the line of sight), location of instantaneous flame front or heat release zone of the combustion zone can be obtained. The important chemical reactions involved in the production of OH radicals and the chemiluminescence intensity are (Gaydon, 1974):



Equations depict a CH radical combine with oxygen molecules to form carbon monoxide and an excited OH* radical. Subsequently, OH* radical at excited state gives chemiluminescence emission and it will reach the ground state.

Chemiluminescence measurement rig consists of an ICCD camera (Nanostar, Lavision) equipped with UV lens (Nikon 105). The frame rate of the camera was 8 Hz. A UG 11 interference filter is used to capture the strong OH* emissions from the A-X (0,0) band (with a peak around $\lambda \approx 310$ nm) and also to suppress the background radiations. The image intensifier is set to an exposure time of $40 \mu s$ to capture the integrated OH* signals. For each burner operating condition, OH* data was acquired for 44 seconds.

3.4 Experimental Procedure

In the cold flow conditions, only dry air was used. In the burner, the desired swirl generator was mounted. The air flow rate (96 Liters per minute) was maintained to ensure Reynolds number of 4000 at the exit of the burner. The flow rate of air was measured using a Coriolis flow meter (Make: Micromotion). Olive oil seeding particles were added to the flow by passing a portion of air through the liquid seeding particle generator. The flow field was shined using double laser pulses. Mie scattered data were acquired in a CCD camera for sufficient duration to obtain the statistical properties of turbulent flow. The same procedure was repeated for other swirl intensities by physically changing the swirl generator.

In the reacting flow studies, the premixed methane-air mixture at stoichiometric condition was supplied to the burner through the inlet ports as shown in Fig. 1. Reynolds number at the exit of the

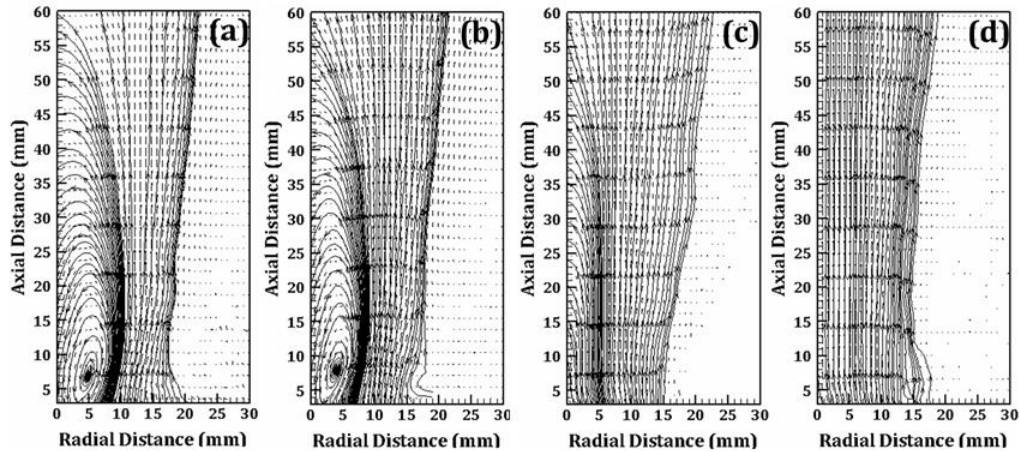


Fig. 3. Streamline superimposed on time mean velocity vector field at different swirl intensity. (a) $S=1$, (b) $S=0.7$, (c) $S=0.4$, (d) $S=0$.

burner at reacting flow condition was also maintained at 4000. A stable flame was anchored. The chemiluminescence emissions from OH^* radicals were imaged using an ICCD camera equipped with a band pass filter for sufficient time for a given swirl generator. Three sets of flow field images were acquired for each swirler. All the experiments for different swirl intensities were conducted at ambient pressure and temperature.

3.5 Post Processing of PIV Data

PIV data was acquired sufficiently long enough to attain statistical time averaged results. The acquired Mie scattered images were processed using DAVIS 8.1[®], a commercial PIV software. In the DAVIS software, the image acquired at the first laser pulse was divided into smaller windows of 32 pixels \times 32 pixels windows with 50% overlap. Spatial cross-correlation technique was applied to each window to identify the displacement of particles within it. The optimum value of duration between each pair of images was arrived to have a maximum particle shift of 4 pixels in a 32 pixels \times 32 pixels window to get a good correlation peak in the present study. The change in the displacement of the particles between the same windows at different time step was obtained and hence the local velocity of each window was obtained. The same procedure was applied for all the acquired pair of images and velocity fields were estimated. The uncertainty in velocity measurement at cold flow conditions depends on several aspects extending from the recording process to the methods of evaluation as summarized in Raffel *et al.* (2000). In the present work, uncertainty was estimated by following the procedure reported by Warda *et al.* (1999a).

3.6 Post Processing of Chemiluminescence Data

As reported in section 3.3, the reaction front of the combustion zone can be identified from the OH^* emissions. In the present work, instantaneous images of line-of-sight integrated OH^* chemiluminescence was recorded for sufficient duration to obtain

statistical time averaged data. The background corrected images contains volumetric intensity data of the axis symmetric flame. Abel inversion was applied to the acquired axisymmetric flame images to de-convolute the 3D data to a planar data. The Abel inversion algorithm reported by Pretzler *et al.* (1992) was used.

4 RESULTS AND DISCUSSION

In this section, the results obtained from cold flow and hot flow are presented and discussed.

4.1 Characteristics of Isothermal Turbulent Flow Field

It is mandatory to address the important characteristics of a swirl flow field such as its local velocity distribution in the measured axial and radial directions, jet spreading rate, energy dissipation and integral length scales. All parameters were estimated for the entire studied operating conditions and are discussed in the following sections.

Figure 3 (a-d) shows the measured time mean velocity vector field for swirling and non-swirling conditions along with streamlines. The stream lines are estimated from the time mean axial velocity component as $\psi = \int_0^r U r dr$. As the present flow is nearly axisymmetric, the velocity vector fields are shown for one of the sides only. Very close to the burner exit, i.e., $x=0-2$ mm, reflection of laser light from the nozzle burner was observed which also resulted in noise in the recordings. Hence, for all the studied operating conditions, the regime between $x=0-2$ mm was not considered for post processing. It is important to mention here that the y axis in Fig. 3 started from 3 mm. From the figures 3 (a-d) it is clear that as the swirl intensity increased, the size of the recirculation zone also increased showing the corresponding increase in the reverse mass flow rate.

4.2 Time Mean Axial Velocity

Figure 4 shows the time mean radial profiles of normalized axial velocity components at different

axial locations for all studied conditions. All velocity components are non dimensionalized using the area averaged velocity (U_{avg}) calculated from the measured mass flow rate of air. The estimated uncertainty in the measured mean axial velocity component for all present studied conditions was found to be having a maximum of 1.43% of the area averaged velocity U_{avg} . Figure 4 shows that with increase in swirl intensity, an increased decay of value of centerline axial velocity was observed and it originates from the positive pressure gradients in the downstream direction induced by the swirl (Kerr and Fraser 1965)

Other important observations from the Fig. 4 are that: (1) The percentage decay in the value of peak axial velocity obtained from the radial profile at axial location of $x = 3D$ with respect to the peak axial velocity obtained from the radial profile at $x = 0.25D$ are 65%, 55%, 47.2% and 13.5% for $S=1$, $S=0.7$, $S=0.4$ and $S=0$ respectively, (2) For all the three swirling cases in the order of $S=1$, $S=0.7$, $S=0.4$, the location of peak values of axial velocity moves radially outward with increase in axial distance from the exit of the burner which typically describes the spreading of swirl flow. Increase in decaying and radial outward shifting of peak value of axial velocity is observed in the case of stronger swirl flow is because of: (a) increase in width of the flow and the corresponding, increase in the size of recirculation zone, and (b) the air entrainment from the surroundings. Also, it can be interpreted from the above discussion that axial velocity can be modified with the help of swirl to a desired value in order to anchor a flame.

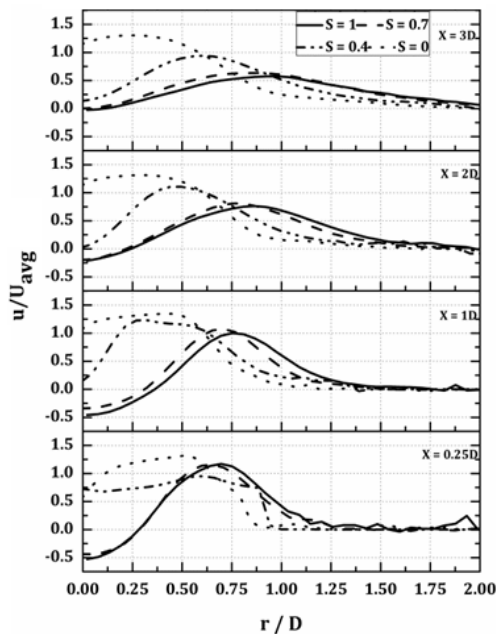


Fig. 4. Non dimensional time mean axial velocity profile at different axial location for different swirl intensity.

4.3 Jet Spreading Rate

As the present burner has an annular exit, jet spread rate was estimated by following sec. 2.1. At an axial

distance, radial locations with 50% value of the peak velocity were obtained. It provided two different radial locations, one close to the axis and another away from the axis. The radial location away from the axis was chosen as mentioned in (Liang & Maxworthy, 2005). Those radial locations at different axial heights were fitted with a straight line. The angle of the fitted straight line with respect to the jet axis was represented as half jet spreading angle ($\alpha_{1/2}$). Figure 5 shows the effect of increase in degree of swirl on the spreading rate of a free swirling jet from present burner at $Re = 4000$. The figure shows that the jet half width angles for different degrees of swirl are as follows: 6.5° for $S = 0$, 8.4° for $S = 0.4$, 9.8° for $S = 0.7$ and 14.2° for $S = 1$. Hence, it is quite clear that spreading angle increased nearly linear with an increase in the geometrical swirl numbers for the present studied axial swirlers. Figure 5 also shows the comparison of jet spread rate with literature data which has similar geometrical swirl number but with different swirl generating methods, i.e., (Chigier & Chervinsky 1967) generated swirling flow by allowing the air through tangential entries, Kerr and Fraser 1965 used axial swirl generators for generating swirl. The agreement between the present values with literature data is good irrespective of different ways of swirl generation and flow conditions.

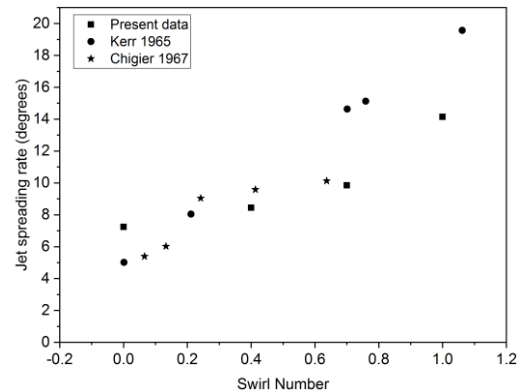


Fig. 5. Comparison of jet spreading angle ($\alpha_{1/2}$) with literature data.

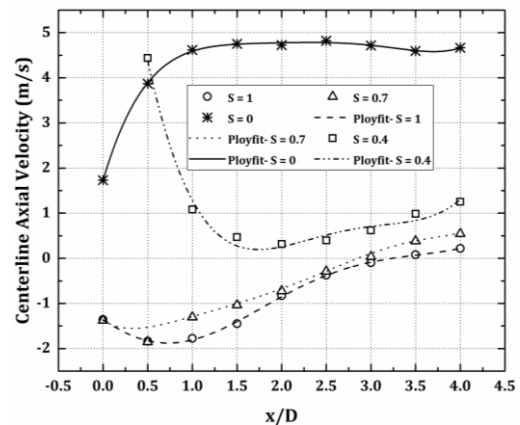


Fig. 6. Non Dimensional centerline velocity verses axial distance for different swirl intensities.

4.4 Recirculation Zone

Figure 6 shows the variation of centreline time mean axial velocity with axial distance from the exit for all studied conditions. For higher degrees of swirl such as 0.7 and 1.0, the axial velocity varies from negative to a positive value and it indicates the presence of reverse flow and the associated recirculation zone. Axial height at which the centerline axial velocity changed from negative to positive is termed as length of recirculation zone (L). The estimated recirculation lengths for $S = 1$ and $S = 0.7$ are $3.4D$ and $3D$ respectively. In the case of $S = 0.4$ and $S = 0$, negative values of axial velocity are not observed at the axis which indicates the absence of recirculation zones. Mass flow rate reversed into the recirculation zone was estimated by following Vanoverberghe and Bulck (2003). Normalized Reverse mass flow rate is calculated using Eq. (6).

$$\frac{\dot{m}_r}{\dot{m}_o} = \frac{\int_0^r 2\pi\rho u_r dr}{\dot{m}_o} \quad (6)$$

where r represents the width of the recirculation zone. For swirl numbers of 0.7 and 1, the estimated normalized reverse mass flow rate is calculated as 0.027 and 0.058 respectively. The amount of mass reversed into the recirculation zone at a given axial distance is more for higher swirl number than lower swirl number. From this, it can be reported that for the present burner configuration at a given Reynolds number, increase in geometrical swirl number from 0.7 (38°) to 1 (50°), i.e., 24% increase in the flow deflection angle, nearly doubled the value of reversed mass flow rate.

4.5 Turbulent Velocity Fluctuations

Figure 7 shows the radial profile of normalized rms axial velocities at different axial locations for different swirl conditions. From the figure, it can be noticed that at $x = 0.25D$, there are two peaks of normalized rms axial velocity present in all swirling cases and a single peak in non-swirling case. The peak value observed close to axis corresponds to inner or wake shear layer whereas another peak away from axis corresponds to outer or jet shear layer. Because of the presence of vortex core in swirling flows, the amplitude of rms axial velocity (u') in the inner shear layer is considerably larger than the outer shear layer. So, the effect of turbulence is very high in the inner shear layer than the outer shear layer for high swirl case which indicates possibility of rapid mixing near inner shear layer than outer shear layer. With increase in axial distance, the magnitude of u' in the inner shear layer decreased faster than the outer shear layer because of higher turbulence and the associated dissipation.

In the present study, the magnitude of time mean radial velocities was also calculated and it was significantly lower than its axial counterparts whereas in the case of fluctuation components, the amplitude of radial fluctuation component (v') was comparable to that of with axial component of fluctuation (u'). It shows the importance of resolving turbulent flow field in all space coordinates. In the present work, only planar

information was recorded and hence the tangential component (w') could not be resolved.

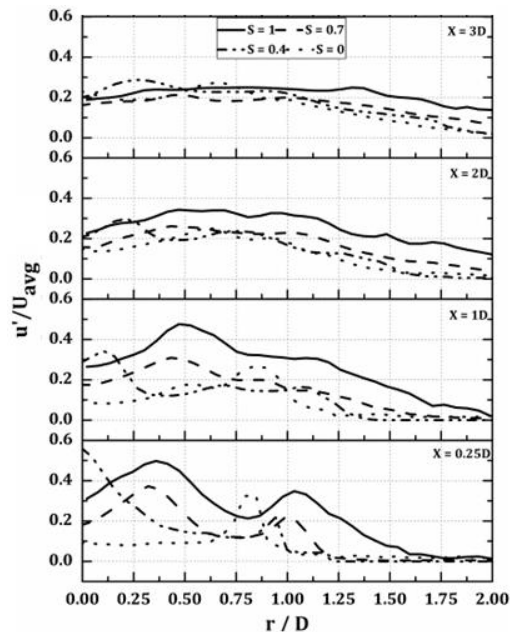


Fig. 7. Radial profile of non dimensional rms axial velocities at various axial locations for different swirl intensities.

4.6 Length Scales

The procedure to estimate integral length scale is reported in section 2.2. Information on length scale is important as it can be used for classifying the premixed turbulent flames. The changes of normalized length scales with the normalized axial distance for different degrees of swirl are shown in Fig. 8. The length scale information was plotted only up to an axial distance of $2D$ due to the fact that velocity field was not disturbed by the ambient air entrainment and mixing in this zone will affect the combustion zone too. For $S = 1$, the values of integral length scales were in the range of $0.1D$ to $0.18D$. For $S = 0.7$, integral length scale over the axial distance till $2D$ fluctuates in and around $0.1-0.15D$. For $S = 0.4$, the integral length scale fluctuates around $0.1D$. As the exit Reynolds number was same for all the conditions, the only variation was due to the difference in the swirl number. Close to the axis, integral length scales for all the cases were smaller and then it increase with increase in axial distance due to the decrease in turbulence with distance because of dissipation. In the non-swirling case, the trend changed completely. The length scale is smaller at the exit and it increases till $x = 2D$ and thereafter it remains nearly constant in the studied domain.

4.7 Reaction Flow Study

To study the effect of swirl on the stability of the flame with respect to anchoring, experiments on reacting flow were conducted for all the operating conditions investigated at isothermal conditions. The air was replaced with combustible mixture

comprised of methane (99.5% purity) and dry air (21% O₂ + 79% N₂ by volume). Velocity field was not measured at reacting flow conditions. Only OH* chemiluminescence emissions from the flame were recorded using an ICCD camera. Important results and the associated inferences are discussed in this chapter.

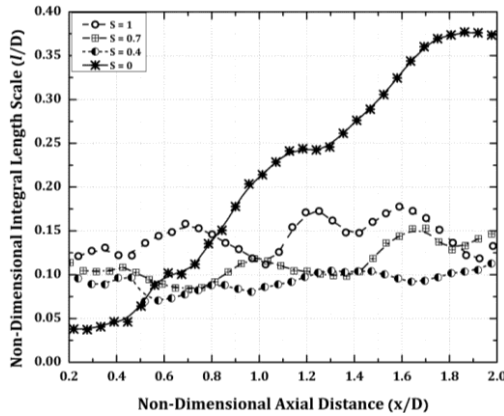


Fig. 8. Normalized integral length scale vs. normalized axial distance for different swirl intensities.

4.8 Lean Blow Out

The spatial distributions of OH* chemiluminescence intensities of stoichiometric methane air turbulent flames recorded at different swirl numbers are shown in Fig. 9. Figure 9 clearly shows that with increase in swirl intensity, the flame spreading rate increased which indicates: (a) an increase in the size of the recirculation zone, (b) an increase in the reverse flow of burnt products towards the fresh unburned gas reactants and (c) an increase in the mixing of hot products and reactants resulting in intense burning.

Lean blow out (LBO) measurements were conducted by anchoring flame at stoichiometric condition. Later, by keeping constant flow rate of air, fuel flow rate was systematically decreased until the blowing out of flame. Surprisingly, equivalence ratios at which LBO attained are 0.62 for S=1, 0.6 for S=0.7 and 0.58 for S=0.4. Low swirl flame could sustain lean mixture conditions because of less entrainment of atmospheric air into reaction zone.

4.9 Estimation of Turbulent Burning Velocity

Reacting-flow PIV measurements were not performed, and hence, the respective flow field data at reacting conditions was not available. In earlier works by Abdel-Gayed and Bradely (1981), Klimov (1981), and Kobayashi *et al.* (1996), turbulent burning velocity was correlated with RMS axial velocity fluctuation measured at cold flow conditions. Hence, a similar approach was followed to estimate possible turbulent burning velocity from cold flow data. The correlation given in Klimov (1981) shown in Eqn 8 was used.

$$\frac{S_T}{S_L} = 3.5 \left(\frac{u'}{S_L} \right)^{0.67} \quad (6)$$

u' is turbulent intensity of isothermal flow at the location of reaction zone and S_L corresponds to laminar burning velocity of stoichiometric methane air mixture obtained from Hermanns *et al.* (2010). So, the obtained turbulent burning velocity of premixed methane air turbulent flames at stoichiometric condition are 4 m/s ($S = 1$), 3.3 m/s ($S = 0.7$) and 3.2 m/s ($S = 0.4$). Above information also clearly states that for a given exit Reynolds number, the exit turbulence field can be modified by altering the swirl intensity and the flame can be anchored at the desired location.

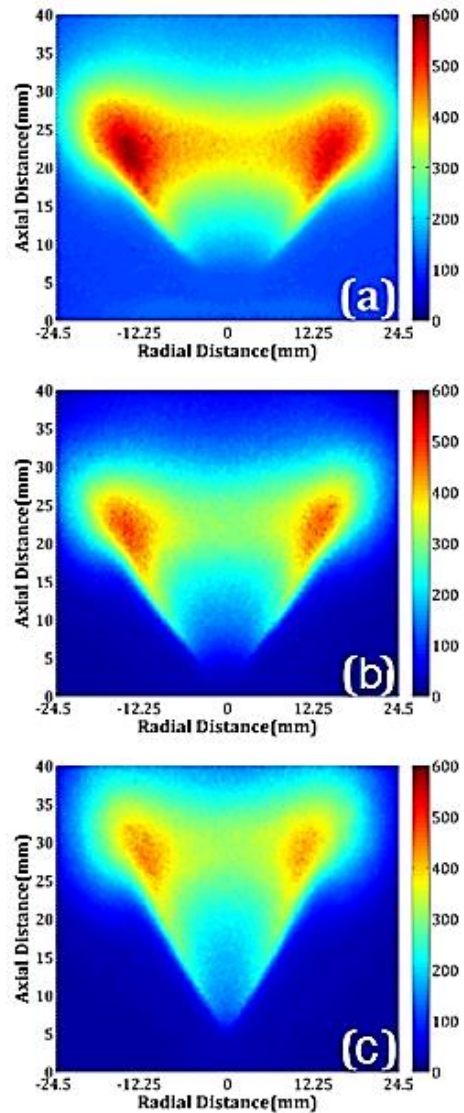


Fig. 9. Time mean OH* chemiluminescence of stoichiometric methane air flames for S=1, 0.7 and 0.4 at T=298 K and P=1bar.

5 CONCLUSION

Effect of swirl on the flow field at the exit of an annular swirl burner was successfully investigated. Two dimensional velocity field was measured using PIV technique at isothermal conditions.

Three axial vaned swirl generators having swirl intensities of 1, 0.7 and 0.4 were investigated. Reynolds number at the exit of the burner was kept constant at 4000. The percentage of decay in the magnitude of peak value of axial velocity obtained from the radial profile at a height of 4D with respect to 0.25D from the burner exit was 65%, 55%, 47.2% and 13.5% corresponding to the swirl intensity of 1, 0.7, 0.4 and 0. Recirculation zones were observed for swirl numbers of 0.7 and 1. The recirculation zone increased with increase in swirl number from 0.7 to 1.0 and the respective length of recirculation zones were 3D and 3.4D. The magnitude of turbulence intensities at wake shear layer was much higher than the jet shear layer due to the presence of reverse flow for $S=0.7$ and 1.0. Experiments with reacting flow indicated that the equivalence ratios at which the lean blow conditions observed were 0.62 for $S=1$, 0.6 for $S=0.7$ and 0.58 for $S=0.4$. Turbulent burning velocity estimated from isothermal turbulence intensity and laminar burning velocity at stoichiometric condition was estimated and it was 4 m/s ($S=1$), 3.3 m/s ($S=0.7$) and 3.2 m/s ($S=0.4$) respectively.

ACKNOWLEDGEMENTS

We sincerely thank Department of Space, India for their financial support. We thank Dr. V. Aravind for his consent to use PIV test rig. We also extend our thanks to Mr. Dinesh, Mr. Vinil and Mr. Bipin for their support during experiments.

REFERENCES

- Abdel-Gayed, R. G. and D. Bradely (1981) A Two-Eddy Theory of Premixed Turbulent Flame Propagation. *Philosophical Transactions of the Royal Society of London* 301, 1-25
- Alekseenko, S. V., V. M. Dulin, Y. S. Kozorezov, D. M. Markovich, S. I. Shtor, M. P. Tokarev (2011) Flow structure of swirling turbulent propane flames. *Flow Turbulence Combust* 87, 569–595
- Beér, J. and N. Chigier (1983) Combustion Aerodynamics. Robert E. Krieger, Malabar, FL
- Bruno, C., and M. Losurdo (2007). The trapped vortex combustor: An advanced combustion technology for aerospace and gas turbine applications. *Advanced Combustion and Aerothermal Technologies*, 365-384.
- Chigier, N. A. and J. M. Beér (1964). Velocity and static-pressure distributions in swirling air jets issuing from annular and divergent nozzles. *Journal of Fluids Engineering* 86,788-796.
- Chigier, N. A., A. Chervinsky (1967). Experimental Investigation of Swirling vortex Motion in Jets. *Journal of Applied Mechanics*, 443-451.
- Gaydon, A. G. (1974) *The spectroscopy of flames*. John Wiley and Sons, NewYork, PP.1-9, 159-163
- Hermanns, R. T. E., A. A. Konnov, R. J. M. Bastiaans, L. P. H. de Goey, K. Lucka, H. Köhne (2010) Effects of temperature and composition on the laminar burning velocity of $\text{CH}_4+\text{H}_2+\text{O}_2+\text{N}_2$ flames. *Fuel* 89,114–21.
- Kerr, N. M. and D. Fraser (1965) Swirl effect on axisymmetrical turbulent jets. *Journal of the Institute Fuel* 38: 519–526.
- Kilik, E. (1976) *The influence of swirler design parameter on the aerodynamics of the downstream recirculation region*. Ph. D thesis. School of Mechanical Engineering, Cranfield Institute of Technology, England
- Kim, H. S., V. K. Arghode, A. K. Gupta (2009) Flame characteristics of hydrogen-enriched Methane–Air premixed swirling Flames. *International Journal of Hydrogen Energy* 34, 1063-1073
- Klimov, A. M. (1981) Premixed Turbulent Flames-interplay of hydrodynamic and chemical phenomena. 8th ICOGER, 23-26
- Kobayashi, H., T. Tamura, K. Maruta, T. Niioka, F. Williams (1996) Burning Velocity of Turbulent Premixed Flames. In A High pressure Environment. 26th symp (International) on combustion. 389-396
- Kojima, J., Y. Ikeda, T. Nakajima (2005) Basic aspects of OH(A), CH(A), and C2(d) chemiluminescence in the reaction zone of laminar Methane-Air premixed flames. *Combustion and Flame* 140, 34-45
- Liang, H., T. Maxworthy(2005). An experimental investigation of swirling Jets. *Journal of Fluid Mechanics* 525, 115–159
- Pretzler, G., T. Neger, H. Philipp, and Woisetschläger, J., Naturforsch, Z. A. (1992) *Physical Sciences* 47: 955–970
- Raffel, M., C. E. Willert, S. T. Wereley, J. Kompenhans (2000) *Particle Image Velocimetry – A Practical guide*, Springer Berlin Heidelberg New York, Second Edition, pp. 164–176
- Singh, S., S. Chander (2014) Heat transfer characteristics of dual flame with outer swirling and inner non-swirling flame impinging on a flat surface. *International Journal of Heat and Mass Transfer* 77, 995–1007
- Syred, N., N. A. Chigier, J. M. Beér (1971). Flame stabilization in recirculation zones of jets with swirl. *Thirteenth Symposium (International) on Combustion* 13, 617-624.
- Turns, S. R. (2000) *An introduction to combustion: concepts and applications*, McGraw Hill Companies, Inc., U.S.A., 2nd edition
- Vanierschot, M., E. Van den Bulck (2008). Influence of swirl on the initial merging zone of a turbulent annular jet. *Physics of Fluids* 105104-1-10

- Vanoverberghe, K. P., E. V. Van Den Bulck (2003) Confined Annular Swirling Jet Combustion. *Combustion Science and Technology* 175, 545-578
- Warda, H. A., S. Z. Kassab, K. A. Elshorbagy, E. A. Elsaadawy (1999a) An experimental investigation of the near-field region of free turbulent round central and annular jets. *Flow Measurement and Instrumentation* 10, 1-14.
- Warda, H. A., S. Z. Kassab, K. A. Elshorbagy, E. A. Elsaadawy (1999b). An experimental investigation of the near-field region of a free turbulent coaxial jet using LDA. *Flow Measurement and Instrumentation* 10, 15-26.